AAS 25-283

LOW-ENERGY TRANSFERS TO QUASI-HALO ORBIT IN A SUN-PERTURBED ENVIRONMENT

Claudio Toquinho Campana[*], Francesco Topputo[†]

Interest in the exploitation of the cislunar environment is growing tremendously. This paper explores the process of designing exterior, multi-impulse Earth-to-Halo transfers within a Sun-perturbed environment. Initial trajectories, generated using fundamental concepts of dynamical systems theory, are optimized and made compliant to the case study. The cost to insert into a Quasi-Halo trajectory is then investigated. Analysis of the results allows inferring relations between design parameters. As a new era of lunar exploration approaches, this work proposes a practical approach for designing efficient cislunar transfers to strategic orbits.

INTRODUCTION

Interest in the cislunar environment and the vast possibilities its exploitation offers is increasing rapidly. The establishment of lunar outposts and orbiting gateways is crucial for enabling the next generation of human exploration in the solar system. Recently, several missions have been launched to our natural satellite, including ArgoMoon,[1] CAPSTONE,[2] EQUULEUS,[3] and Chang'e-6. Additional missions are planned for the near future, and it is clear that the cislunar domain will soon become a strategic highway for thousands of spacecraft.

Designing cislunar transfers is a delicate process. The environment is inherently chaotic, making the phase space complex and preventing dynamic generalization. Specialized astrodynamic models are employed during early mission planning phases to balance complexity and realism.[4] Additionally, simplified dynamic models reveal natural structures, such as periodic orbits and invariant manifolds, that offer a clearer interpretation of certain regions within the dynamic landscape.[5] This opens up the possibility of achieving efficient routes across the system.[6] Once a prototype trajectory is developed, refinement techniques are used to smoothly transition to higher-fidelity models that more accurately represent the real dynamics experienced by a spacecraft.[7,8]

In this work, exterior, multi-impulse cislunar trajectories are designed within a Sun-perturbed environment. The case study involves generating Earth-to-Halo (E2H) transfers and achieving Quasi-Halo (QH) trajectories about the L_2 point of the Earth–Moon (EM) system. Problem constraints are inspired by typical CubeSat missions, where propulsion capabilities and operational limits significantly influence the design process. Initial prototype trajectories are seeded by leveraging the tube dynamics emanating from a Halo orbit in the EM circular restricted three-body problem (CR3BP), followed by propagation in the Sun-perturbed, bi-circular restricted four-body problem (BCR4BP). A nonlinear programming formulation ensures that transfers meet constraints and are propulsively

[*]Ph.D. Student, Dept. of Aerospace Science and Technology, Politecnico di Milano, Via G. La Masa 34, Milano, Italy.
[†]Full Professor, Dept. of Aerospace Science and Technology, Politecnico di Milano, Via G. La Masa 34, Milano, Italy.

efficient. In a second phase, QH trajectories are generated and the cost to insert into these is investigated. The analysis aims to uncover relations between different design parameters. Overall, this work contributes to enhancing understanding and improving design practices for early-stage mission planning within the cislunar environment.

The paper is structured as follows. The first section introduces the dynamic model herein adopted. The procedure implemented to generate E2H transfers and the QH insertion strategy are then presented. Results are shown and discussed, and conclusions are drawn at the end of the paper.

BACKGROUND

Earth–Moon, Sun-perturbed bi-circular restricted four-body problem

In the BCR4BP, the Sun is seen orbiting circularly about the EM system barycenter. This formulation departs from the dynamic representation of the CR3BP due to the inclusion of the solar attraction and the resulting inertial forces. Referring to Figure 1, the equations of motion are formulated in the rotating frame centered at the EM barycenter, with the x axis directed toward the Moon, the z axis perpendicular to the orbital plane of the primaries, and the y axis completing the triad.

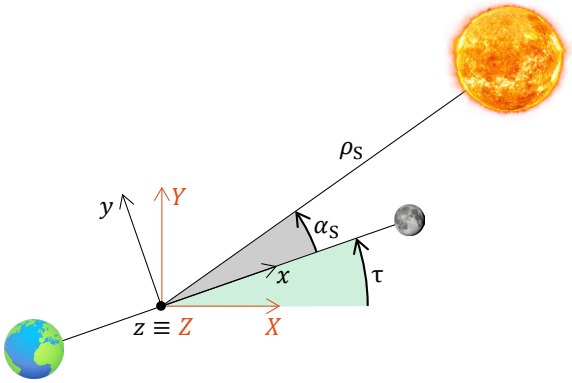

Figure 1: BCR4BP model (not to scale). Non-rotating, quasi-inertial coordinates in orange.

The equations of motion of the BCR4BP read[9]

$$\begin{aligned} \ddot{x} &= 2\dot{y} + \frac{\partial \Omega_4}{\partial x} \\ \ddot{y} &= -2\dot{x} + \frac{\partial \Omega_4}{\partial y} \\ \ddot{z} &= \frac{\partial \Omega_4}{\partial z}, \end{aligned} \tag{1}$$

where

$$\begin{aligned} \Omega_4 \ = \frac{1}{2}(x^2+y^2) + \frac{1-\mu}{r_E} + \frac{\mu}{r_M} + \frac{1}{2}\mu(1-\mu) + \\ + \frac{m_S}{r_S} - \frac{m_S}{\rho_S^2}\left(x\cos(\alpha_S) + y\sin(\alpha_S)\right) \end{aligned} \tag{2}$$

is the effective potential and

$$\alpha_S = \omega_S(\tau - \tau_0) + \alpha_S\big|_{\tau_0} \tag{3}$$

is the instantaneous Sun phase angle in the rotating frame (default value $\alpha_S\big|_{\tau_0=0} = 0°$). The quantity r_i represents the scaled distance of the spacecraft from the ith celestial body. In this representation, the Earth is fixed at $[-\mu, 0, 0]$, whereas the Moon rests at $[1-\mu, 0, 0]$. The non-dimensional values characterizing the dynamic framework are reported in Table 1. If the solar perturbation is neglected, this model reduces to the CR3BP.

Table 1: Non-dimensional BCR4BP physical parameters.

Symbol	Value	Description
μ	$1.215\,066\,830 \times 10^{-2}$	Mass parameter
m_S	$3.289\,005\,410 \times 10^{5}$	Sun mass
ρ_S	$3.888\,111\,430 \times 10^{2}$	EM–S distance
ω_S	$-9.251\,959\,850 \times 10^{-1}$	Sun angular velocity

METHOD

This section formalizes the process developed to design E2H transfers in the BCR4BP and the subsequent QH insertion phase. The proposed approach foresees dividing a full Earth-to-QH trajectory into two segments, each optimized individually and independently. First, dynamical systems theory is adopted to seed solutions that asymptotically reach the destination Halo. Further back-propagation in the BCR4BP permits identifying all those trajectories approaching the vicinity of the Earth in a reasonable amount of time. Then, a nonlinear programming problem is formulated to achieve feasible and optimized E2H transfers. A second paragraph describes the QH generation and insertion strategy necessary to complete the design of the trajectories.

Earth-to-Halo transfer phase

Moon approaching phase. The spacecraft is assumed to target a Halo orbit about the L_2 point of the EM system, with Jacobi energy equal to 3.09. The case study takes inspiration from the LUMIO mission, a CubeSat that will perform an exterior transfer to the mentioned Halo.[10] The third order Lindstedt-Poincaré approximation guesses good initial conditions of the target orbit in the CR3BP. A continuation scheme based on a single shooting approach permits converging to the desired Halo.

Dynamical systems theory suggests that stable and unstable invariant manifolds arise from periodic orbits about Lagrange points.[11] These can be generated by slightly perturbing the conditions along the orbits themselves. At this purpose, the monodromy matrix, that is, the state transition matrix after one orbit revolution over the reference periodic solution, is computed. The spacecraft shall approach the Halo orbit from afar of the EM system. Therefore, the right stable manifold is computed by perturbing the orbital states along the local stable eigenvector directions and back-propagating until crossing the EM region of prevalence (ROP). The EM ROP is the imaginary surface that bounds the region where the dynamics of the BCR4BP can be accurately approximated by the CR3BP, in practice disregarding the presence of the Sun.[12] Figure 2 depicts the right stable manifold of the destination Halo orbit, back-propagated until the EM ROP crossing.

Trajectories seeding. Terminal states of each manifold trajectory are further propagated backward, this time in the BCR4BP. As the model is non-autonomous, the Sun–Earth–Moon relative configuration along the trajectory is relevant. To account for this important property, eight different geometries are considered at the time the spacecraft departs backward the EM ROP in the BCR4BP. In particular, the Sun angle $\alpha_S\big|_{\tau_{ROP}}$ is varied between 0° to 360° with an angular discretization of

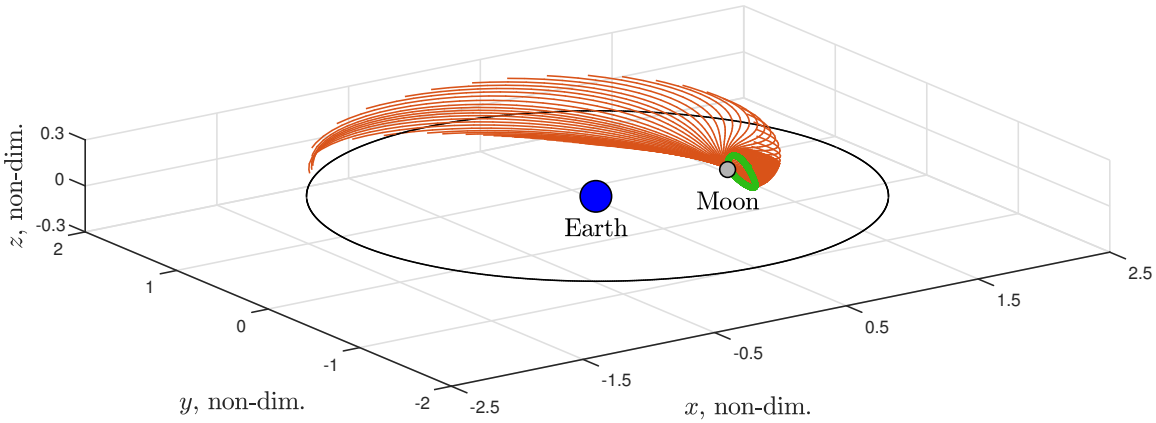

Figure 2: Right stable manifold (orange) approaching the destination Halo orbit (green) in the CR3BP. The EM ROP circle is projected onto the synodic plane.

45°. The propagation stops either when the spacecraft reaches the vicinity of the Earth at a threshold distance from its center of 2/3 non-dimensional units that, roughly, corresponds to 2/3 the real EM distance, or after a maximum propagation time of 100 days. A filter removes all trajectories showing complex geometries when represented in the synodic frame (e.g., multiple Earth revolutions close to its surface), thus retaining only solutions that are meaningful for the purpose of this study.

Earth-to-Halo optimization. Prototype trajectories approaching the vicinity of the Earth within the admissible propagation time serve as guesses fed to the optimization algorithm. Objective functions and constraints are introduced to simulate a real CubeSat space mission, thereby accounting for technological limits and operational restraints. The optimization problem is solved through direct transcription and multiple shooting.[13]

To generate a multi-impulse E2H transfer, a seeding trajectory is sampled at some discrete nodes. The discretization is function of the number of maneuvers (NoM), input parameter of the process. As the transfer is supposed to leave the Earth and insert into the destination Halo orbit impulsively, $NoM - 1$ equally-spaced ballistic arcs are generated. To introduce additional freedom to the problem, the boundary epochs of all arcs are considered optimization variables. The generic jth arc is further sampled at K nodal points, each couple defining a segment. During optimization, this precaution helps reducing sensitivity to the chaoticity of the dynamics and favors convergence to a feasible solution. The objective function to be minimized reads

$$\mathcal{J} = \sum_{i=2}^{NoM} \left\| \boldsymbol{\Delta V}_i \right\|. \tag{4}$$

Prior to the trans-lunar injection (TLI) maneuver, the spacecraft is assumed to be orbiting a 167 km altitude circular Low Earth Orbit (LEO). The TLI impulse does not contribute to the computation of the cost function, as it is provided by the last stage of the launcher. The expense of an intermediate deep-space maneuver (DSM) is obtained by computing the Euclidean norm of the velocity difference across the respective couple of arcs. The last maneuver describes the cost that would be necessary to insert at any point of the destination Halo orbit. However, as the optimization is carried out in the BCR4BP, without further control the spacecraft would leave the Halo after a short period of time because of the solar perturbation. This concept is explored in the next paragraph. A schema of the overall multiple-burn, multiple shooting method is shown in Figure 3.

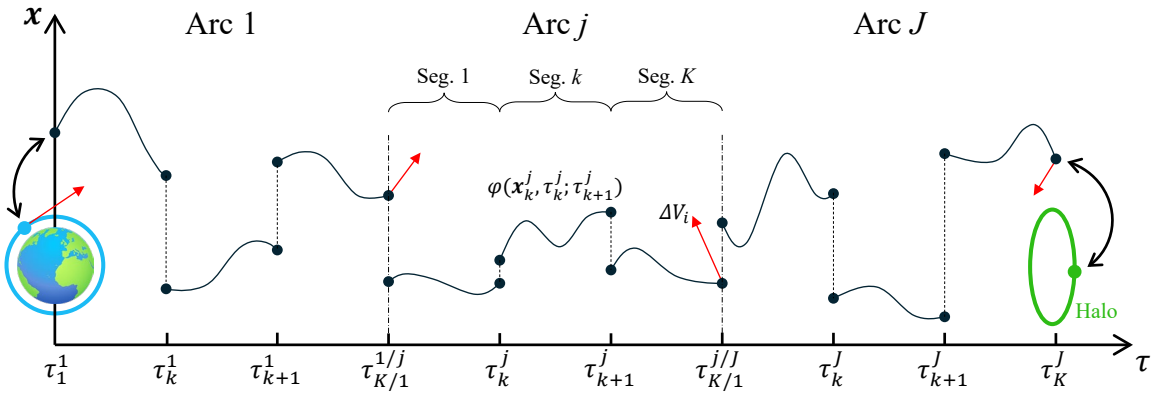

Figure 3: Multiple-burn, multiple shooting schema.

Constraints are introduced to the formulation to achieve transfers that are compliant with mission requirements. In particular, equality constraints

$$\begin{aligned}(x_1^1+\mu)^2+(y_1^1)^2+(z_1^1)^2-r_{\text{dp}}^2&=0\\(x_1^1+\mu)\,\dot{x}_1^1+y_1^1\,\dot{y}_1^1+z_1^1\,\dot{z}_1^1&=0\end{aligned} \tag{5}$$

force the spacecraft to depart tangentially the LEO (with r_{dp} representing the target non-dimensional distance from the center of the Earth). The insertion into the destination Halo orbit is modeled as

$$\begin{bmatrix}x\\y\\z\end{bmatrix}_K^J = \begin{bmatrix}x\\y\\z\end{bmatrix}_{\in\text{Halo}}, \tag{6}$$

connoting that the position of the last node of the transfer must match any position triad belonging to the hypothetical Halo orbit that one would achieve if the dynamics reduced to the CR3BP. To parameterize this one, cubic interpolation splines are derived as a function of the angle θ swept between the xz plane of the EM synodic frame and each point along the Halo orbit itself, positive clockwise (0° at perilune). This angle identifies an additional optimization variable of the problem. Ballistic continuity of the trajectory between nodal points within an arc is enforced by

$$\boldsymbol{\xi}_k^j = \boldsymbol{\varphi}(\boldsymbol{x}_k^j, \tau_k^j; \tau_{k+1}^j) - \boldsymbol{x}_{k+1}^j = 0, \tag{7}$$

where $\boldsymbol{\varphi}(\boldsymbol{x}_k^j, \tau_k^j; \tau_{k+1}^j)$ represents the flow of the (j,k)th segment of the trajectory propagated in the target BCR4BP dynamics. Across two generic adjacent arcs, continuity is prescribed by the matching of the position only, as an impulsive maneuver is admitted and the instantaneous velocity can vary. Additional equality constraints are imposed thus ensuring time continuity between arcs.

To conclude the formulation, inequality constraints prevent the spacecraft from impacting with either primary at the discretization points and model operational and technological limits. In particular, a minimum time interval of 7 days between consecutive maneuvers is foreseen to permit navigation and tracking routines. Furthermore, all intermediate impulses are limited in magnitude to 50 m/s. The final maneuver, necessary to match the velocity of the Halo orbit at the arrival point, is forced to cost less than 5 m/s, as the objective is to exploit the tube dynamics and achieve a transfer that approaches the periodic orbit almost asymptotically. Finally, the total propulsive expense,

ignoring the first impulse at LEO provided by the launcher, is bounded to maximum 200 m/s. The gradient of the objective function and the Jacobians of the constraint equations are provided analytically to the optimizer to enhance computational efficiency.

Quasi-Halo orbiting phase

All optimized E2H transfers resulting from the previous phase are further manipulated to derive QH insertion sections. This paragraph describes the procedure implemented to generate QH trajectories first, and then the method for inserting into them.

Quasi-Halo generation. In general, Halo orbits associated to collinear Lagrange points originate when the dynamics reduces to that of the CR3BP. If particular resonance conditions are not matched, additional perturbations disrupt their periodicity. However, the periodic nature of the BCR4BP enables the generation of quasi-periodic orbits in the vicinity of resonant solutions. Therefore, many CR3BP periodic orbits have dynamically equivalent quasi-periodic trajectories in this higher-fidelity model.[14] In particular, as the number of non-commensurate fundamental frequencies raises to two, infinite quasi-periodic solutions exist, and they evolve on two-dimensional tori. The first fundamental frequency is constrained to be commensurate with the synodic period of the system, whereas the second is free and distinguishes between different quasi-periodic families.

In the literature, techniques have been refined to compute two-dimensional tori about periodic orbits.[15–17] However, in this research, QH trajectories are generated following a procedure developed to derive dynamical substitutes of Lagrange point orbits.[18] This is necessary to account for the fact that the synodic solar angle at the end of a E2H transfer results from the previous optimization, and may not match the Sun angle of the corresponding invariant curve one would obtain on the ideal two-dimensional torus. Therefore, in this work, QH trajectories are intended as solutions that remain in close proximity to the Halo orbit for a certain number of revolutions. To numerically compute a trajectory, multiple revolutions over the ideal Halo orbit are stacked together to create the seeding guess to a nonlinear programming optimization problem. At this purpose, the arrival position of a E2H transfer trajectory is extracted and the $\theta\big|_{\mathcal{T}_{\text{Halo}}}$ and $\alpha_{\text{S}}\big|_{\mathcal{T}_{\text{Halo}}}$ angles are evaluated. Starting from this terminal condition, four complete orbital revolutions are stack together forward in time to cover for an orbiting time of approximately 50 days. An additional revolution is added before to facilitate the optimization process and the quality of the resulting trajectory.

A nonlinear programming problem is formulated. The seeding trajectory is sampled at K nodal points. Continuity across nodal points is enforced similarly to before, as per Eq. (7), so that obtaining a motion that satisfies the dynamics of the BCR4BP. No other constraints are introduced. The purpose is to achieve a QH trajectory that strongly preserves dynamical features, such as longitudinal frequency and geometrical characteristics, of the original Halo orbit. Therefore, the objective function requires minimizing the quadratic form of the constraints, i.e.,

$$\mathcal{J} = \frac{1}{2}\boldsymbol{\Xi}^{\top}\,\boldsymbol{\Xi}, \tag{8}$$

where $\boldsymbol{\Xi}$ is the vector grouping all $\boldsymbol{\xi}_k$ residuals. This formulation ensures minimal corrections during multiple shooting optimization. Figure 4 shows an example of Halo-to-QH transformation.

Quasi-Halo transfer and insertion. The QH transfer phase is modeled as a two-impulse section that departs the terminal state of the E2H stage, prior executing its last impulsive maneuver, and inserts into the target QH trajectory. A nonlinear programming problem is formulated similarly to the one conceived for the first transfer phase. In this case, only one arc sampled at some discrete

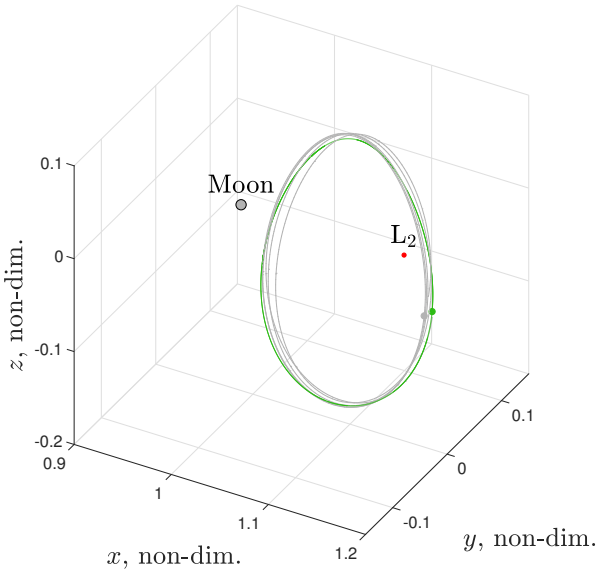

Figure 4: Halo-to-QH transformation. Ideal CR3BP Halo orbit in green, BCR4BP QH dynamical substitute in gray. Dots highlight states at E2H terminal time on both Halo and QH trajectory.

points is considered. The time and position at the first impulse are constrained to match the final ones of the E2H section. The second impulse is forced to happen at a time comprised between 7 days and one Halo period after the beginning of this phase. Continuity in position and velocity between consecutive nodal points is imposed. The terminal position must belong to the target QH, whose states are represented as cubic splines as a function of time, at a suitable epoch to account for the non-autonomous nature of the model. The cost of each impulse is bounded to a maximum of 50 m/s. Gradients and Jacobian matrices are provided analytically for computational efficiency.

As for the previous problems, it is necessary to guess the states at the nodes. The first point corresponds to the terminal state of the E2H section, before the execution of its last maneuver. This precaution is necessary since the terminal impulse of the E2H transfer was optimized assuming to insert into the ideal Halo orbit, irrespective of the fact that only a QH trajectory can be achieved within the BCR4BP framework. All other nodal points are extracted from the interpolating splines sampled at equally-spaced time instants, assuming a time of flight (TOF) of 7 days. The QH transfer phase is optimized by minimizing the total cost of the two maneuvers. The first impulse is computed using the terminal velocity of the E2H section before its final burn.

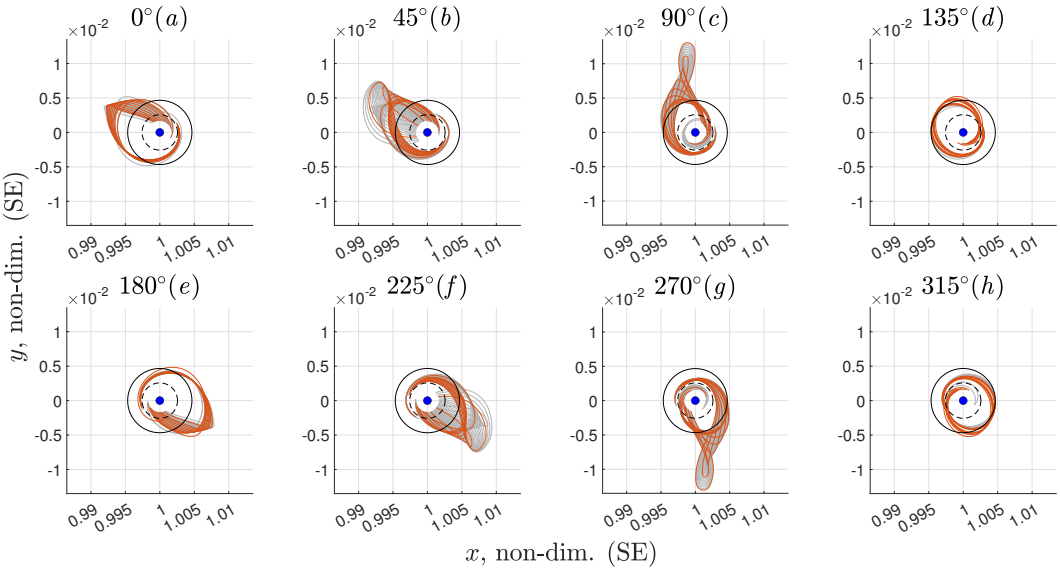

Figure 5: Seeding trajectories projected onto the SE rotating frame. Tiles correspond to different Sun–Earth–Moon configurations at ROP crossing. Black circle indicates EM ROP, whereas dashed line marks lunar orbit. Orange solutions are subject to nonlinear programming optimization.

RESULTS

In this section, the method devised above is applied to produce low-energy QH transfers. First, the E2H legs are generated. The QH insertion segments are consequently optimized. A critical analysis of the results is presented.

Earth-to-Halo transfers design

Seeding trajectories shaping. As previously discussed, E2H transfers are generated starting from seeding guesses that are obtained by back-propagation of the stable manifold of the destination Halo orbit. Figure 5 reports all trajectories derived in this phase. Solutions are projected onto the xy plane of the Sun–Earth (SE) rotating frame, that is, the CR3BP-equivalent frame of reference for the SE system. A simple transformation permits expressing the original states in this new representation. Each tile reproduces a different Sun–Earth–Moon configuration at the time the spacecraft departs backward from the EM ROP, with titles indicating $\alpha_S\big|_{\tau_{ROP}}$ angles and family labels. Ten trajectories are extracted and highlighted in orange in the figure per each configuration. These trajectories are subject to the successive optimization process. In a forward vision, all trajectories depart from the vicinity of the Earth and approach the Halo orbit near to the Moon, whose orbit is represented by the dashed circle. Several trajectories, especially those belonging to families *d* and *h*, experience an intermediate lunar flyby immediately after departure. Furthermore, as evidenced, exterior transfers in the BCR4BP take place when the apogee lies either in the second or fourth quadrant of the SE frame.[19] Thus, numerical results align with theoretical considerations.

Optimization of extracted trajectories. Trajectories highlighted in Figure 5 are optimized. Each seed is processed six times where, at each occurrence, the NoM is incremented from 3 up to 8. The nonlinear programming formulation seeks for the minimization of the payload total transfer cost, that is, the cost without the first impulse provided by the launcher (i.e., the TLI maneuver).

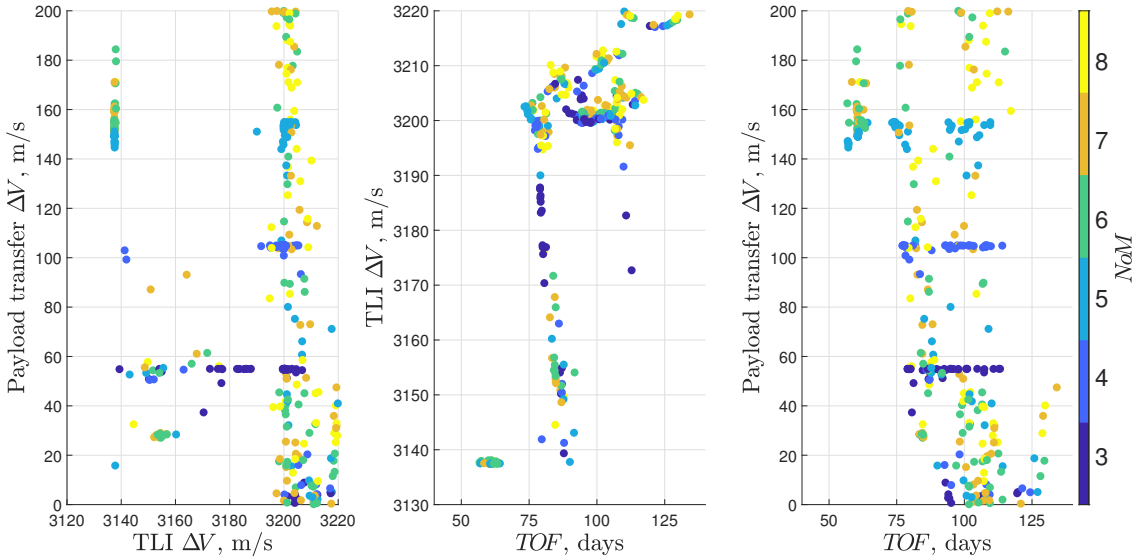

Figure 6: Performance analysis of optimized E2H transfers.

Figure 6 relates important performance indexes of the transfers converging to feasible solutions after multiple shooting optimization. The first two tiles on the left show that the variability in TLI cost is very limited for all transfers, with an average value of 3185.61 m/s. Solutions presenting an injection ΔV smaller than 3190 m/s exploit an intermediate lunar flyby. Among those, transfers lasting about 60 days belong to families *d* and *h* in Figure 5, whereas transfers experiencing longer durations are of families *b*, *c*, *f*, and *g*. Transfers with 3 to 5 maneuvers emerge as clusters in the first and third tiles. Since those transfers require 1 to 3 DSMs, the optimization routine converges to solutions that consume almost the total admissible ΔV, i.e., 55, 105, and 155 m/s, respectively. As the number of DSMs increases, trajectories distribute more evenly in terms of payload ΔV to conform to the maximum allowable cost of 200 m/s. Figure 7 plots the transfer whose cost is the cheapest from the payload perspective, projected onto different frames. The optimization of the seeding trajectory leads to a E2H transfer lasting 101.72 days, and implies, besides departure and insertion maneuvers, four intermediate impulses. Since the total propulsive cost of the spacecraft equals 0.14 m/s, this transfer can be considered almost ballistic. TLI maneuver by the launcher requires 3210.95 m/s. Figure 7c, that is, the representation in the Earth-centered, quasi-inertial frame (ECqi), evidences that DSMs are performed close to the apogee of the transfer. Efficiency is thus achieved by firing close to the apoapsis, where a small impulse results in significant variations in the trajectory. This behavior is common in almost all converging cases. Figure 7d shows that the original seed belongs to family *e*, whilst its optimized version resembles a solution that can be classified in between families *f* and *g* (ROP crossing moves to $\alpha_S\big|_{\tau_{ROP}} = 248.71^\circ$ after optimization).

Keplerian elements in the ECqi are calculated. Almost all transfers experience a prograde departure, with average inclination with respect to the synodic plane of 18.15°. Geometric departure conditions are reported in Figure 8. In particular, the plots relate synodic longitude and latitude relative to the center of the Earth, initial solar angle, and family label. Distinct families of solutions seem to prefer specific longitude and latitude ranges. It is especially the case for families *d* and *h*, that require precise departure geometries to achieve effective lunar flybies. Indeed, the inset in the first tile highlights that favorable conditions for this type of transfer are attained when departing

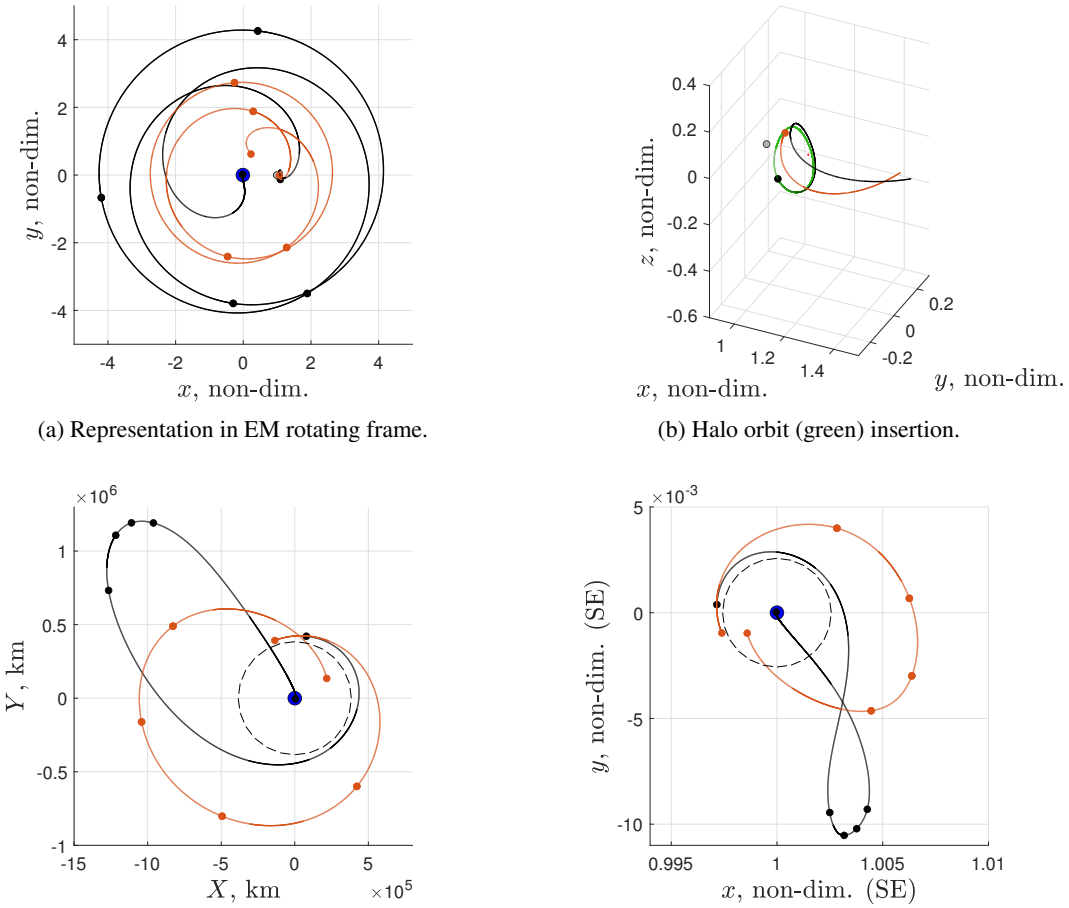

(a) Representation in EM rotating frame.

(b) Halo orbit (green) insertion.

(c) Representation in ECqi frame.

(d) Representation in SE rotating frame.

Figure 7: Most efficient transfer from payload standpoint. Orange trajectory is the seeding solution, whose optimized counterpart is represented in black. Dots mark maneuver points. Dashed line represents lunar orbit.

on a nearly planar trajectory at a synodic longitude of approximately 241°. The tile on the right illustrates that, to generate transfers belonging to different families, a change in departure longitude must correspond to a shift in the instantaneous solar angle, $\alpha_S\big|_{\tau_{dep}}$.

No appreciable relations emerge among the TLI cost, other departure orbital elements, the spacecraft propulsive expense, the NoM, and the original family of belonging. However, the first tile of Figure 9 shows that, generally, there is a connection between the Sun angle at the departure instant from the Earth, the family of origin, and the TOF. This last grows as the Sun angle increases and initial families appear as well distinguished clusters. This, together with the correct synodic longitude at departure, guarantees achieving the proper Sun–Earth–Moon configuration at maximum distance from the EM barycenter, which is fundamental when designing low-energy exterior transfers.

Finally, a clear pattern appear in the second tile of Figure 9, where the insertion angle at the Halo orbit is plotted as function of the Sun angle at the end of each transfer. Families from a to

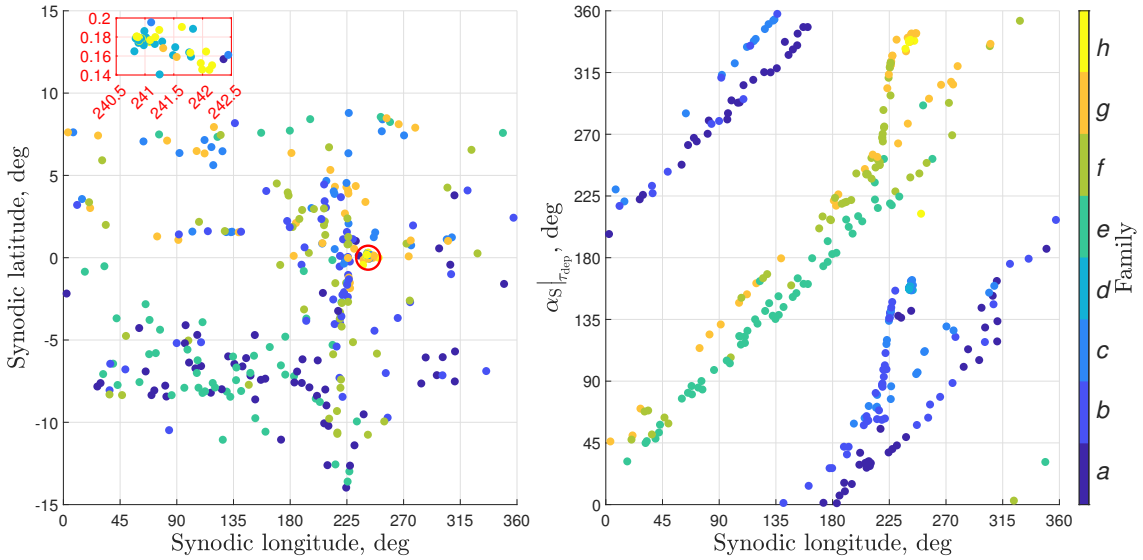

Figure 8: Geometrical analysis at departure from Earth.

d reach the destination orbit when the Sun is at the opposite side of the Moon with respect to the Earth. All other transfers terminate when the Earth, the Moon, and the Sun are aligned respecting this order. Furthermore, each transfer family favors specific ranges of the Halo insertion angle. Figure 10 explains why there are two preferred ranges of Sun angle at arrival time. The last impulse at the terminal state of a transfer serves to inject the spacecraft into the ideal Halo orbit. Figure 10a reports the mean cost and standard deviation of this maneuver, decomposed into its components, computed over all solutions. It appears that the most costly contribution is needed to increase the speed along the x direction. Terminal states before the execution of the last maneuver are used to

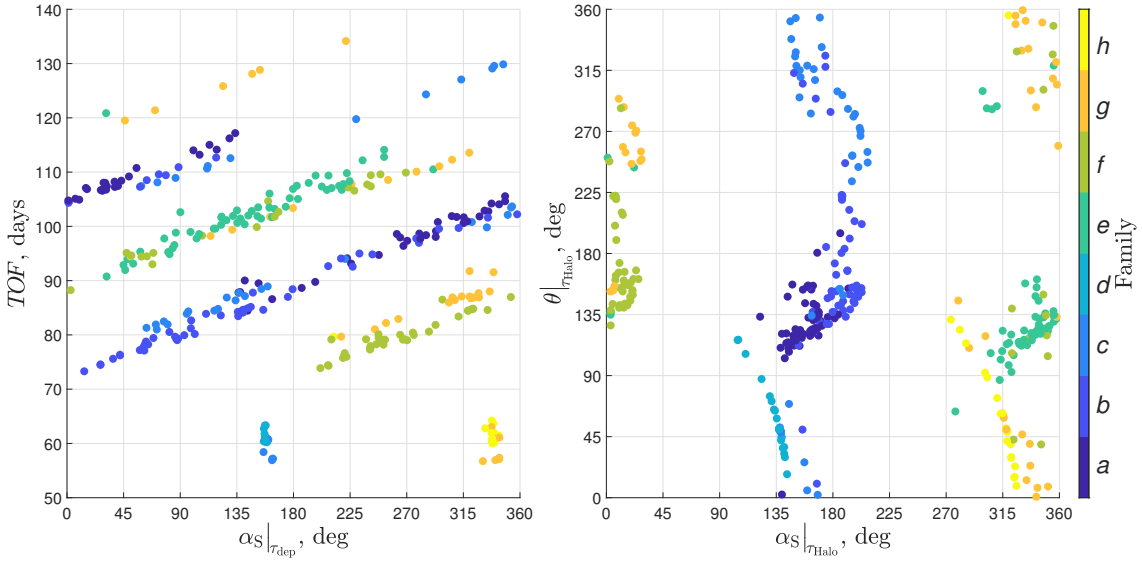

Figure 9: Relations between boundary conditions of E2H transfers.

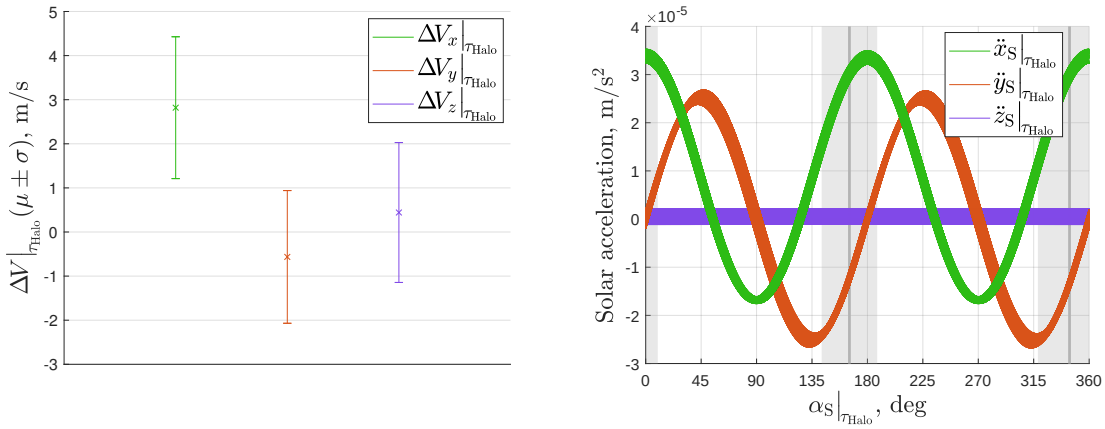

(a) ΔV required to inject into Halo orbit.

(b) Solar perturbing acceleration at arrival time.

Figure 10: Conditions at E2H terminal state.

derive the perturbing acceleration introduced by the Sun as function of its synodic angle, as depicted in Figure 10b. Each curve refer to a specific transfer and, correspondingly, arrival conditions. It is clear that the terminal state of the spacecraft is of little relevance, as the curves overlap. However, the Sun angle in the EM synodic frame is crucial. In this figure, the two vertical lines represent the averages of the two preferred solar angles at arrival time, with light gray areas indicating the associated standard deviations. Comparing the two plots, it is understandable why the optimizer converges to solutions approaching the Halo orbit when the solar angle is slightly ahead of 180° or 360°. To enhance efficiency of the last impulse, it is convenient accumulating positive ΔV on the x direction during the final part of the transfer. On the contrary, a negative variation in speed is beneficial along y. Recalling that the Sun appears to rotate clockwise in the EM synodic frame, optimality is attained when a transfer terminates within either preferred solar angle ranges.

Quasi-Halo insertion

E2H transfers target a perfectly periodic Halo orbit that one would achieve if reducing the dynamics to that of the CR3BP. However, this work assumes a relatively more sophisticated model where the presence of the Sun is no longer neglected. Therefore, since the reference orbit is not in resonance with the characteristic frequency of the system, only QH trajectories can be attained.

All feasible solutions obtained in the previous section provide initial conditions to the final QH transfer phase. As the Sun angle varies making the model non-autonomous, a target QH orbit that is spatio-temporally close to the ideal Halo has to be generated for each specific transfer following the procedure presented before. After that, the multiple shooting algorithm optimizes the two impulses necessary to perform the orbital insertion. Figure 11 shows the cost of the maneuvers necessary to make such transfers. The initial impulses needed to initiate QH transfers seem cheaper for E2H trajectories belonging to families *b* and *f*. On the contrary, families *a* and *e* require higher impulses. It is conjectured that the instantaneous Sun angle at the beginning of this phase is the cause of the disparity. As evidenced in the second tile of Figure 9, transfers associated to families experiencing low propulsive initial cost are those initiating when the Sun is either in the first or third quadrant of the EM synodic frame. Instead, the Sun occupies any remaining quadrant in all other cases. Figure 12 confirms that the Sun angle at the beginning of a long duration QH transfer is determinant

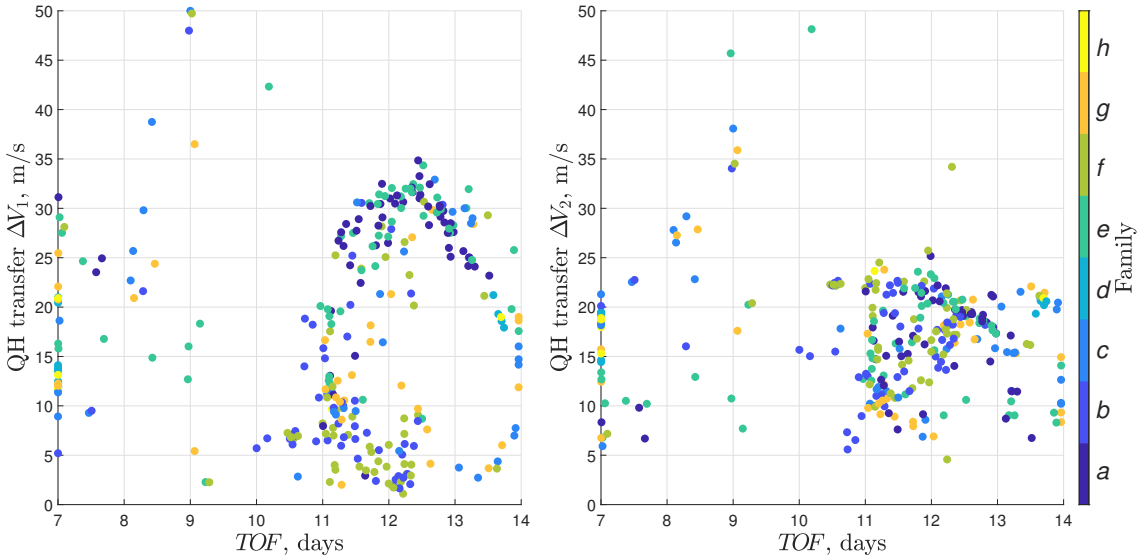

Figure 11: QH transfer and insertion phase. The Sun angle at the beginning of the transfer is decisive in determining the propulsive cost of the first impulse.

in lowering the cost of the first impulse, and consequently the total expenditure. On average, a QH insertion requires 34.64 m/s in total and takes 11.01 days.

An investigation is carried out to deduce the relation between the Sun angle at the time of the first impulse and its cost. As a clear pattern emerges for QH insertions lasting more than 10 days in Figure 12, the following analysis involves those solutions only. Figure 13 shows that the maneuver expense of long lasting transfers resembles a sinusoidal evolution with respect to the solar angle, this happening across 180° and 360°. It is clear, therefore, that a cyclic behavior emerges. The

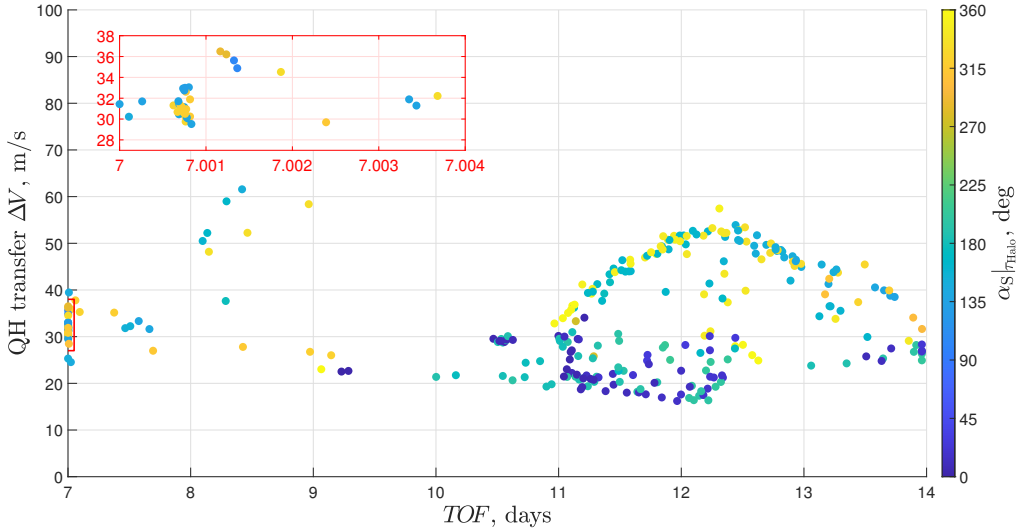

Figure 12: QH transfer total cost as function of the TOF and the initial Sun angle.

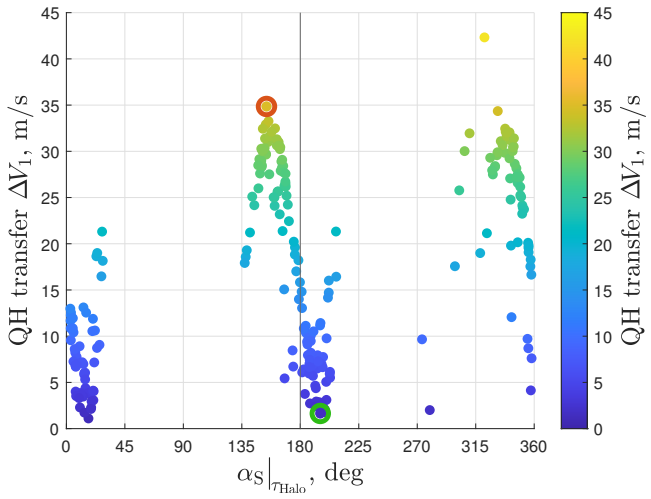

Figure 13: Cost of first impulse to insert into QH transfer as function of the initial solar angle.

two solutions marked with circles are extracted for analysis. They are the upper and lower bounds for ΔV_1 among all solutions departing the ideal Halo orbit with the Sun close to be in opposition with respect to the Earth. Figure 14 depicts the QH insertion phase for both examples. The gray surface in the plots is a torus-like shape that emerges after seeding several quasi-periodic solutions at varying boundary conditions of the optimization problem. In the plots, this 2-dimensional manifold is achieved as follows. First, QH trajectories are originated for several $\theta|_{\tau_{\text{Halo}}}$ and $\alpha_S|_{\tau_{\text{Halo}}}$ couples. As the solar perturbation repeats almost perfectly every 180°, as per Figure 10b, only $\alpha_S|_{\tau_{\text{Halo}}}$ angles ranging from 0° to 180° are considered in this analysis. That is, QH trajectories with solar angles 180° apart at the reference time would be, in practice, nearly identical. For each resulting quasi-periodic orbit, the position at initial reference time is then extracted, similarly to what done in Figure 4. Finally, cubic splines interpolate all reference points associated to a specific solar angle, thus drawing a curve that shadows the evolution of the Halo orbit. Together, these curves produce the torus-like shape depicted in the figures. Given the Halo angle at the end of an E2H section, $\theta|_{\tau_{\text{Halo}}}$, its corresponding "solar circle" is generated by highlighting initial time positions over quasi-periodic trajectories optimized at different solar angles. This circle is traced as a colorful ring, and the point associated to the $\alpha_S|_{\tau_{\text{Halo}}}$ angle at terminal state of the E2H transfer is highlighted over it. The local evolution of the associated QH trajectory, from E2H terminal time to second maneuver epoch, is reproduced and it appears originating from the mentioned point.

The upper tile of Figure 14 plots the QH transfer with the cheaper ΔV_1 among the two solutions. The blue dot, representative of the solar angle at the time of first impulse, marks the point where the local quasi-periodic orbit departs, with a value of 195.38° (the "solar circle" repeats almost identically every 180°). The entire insertion phase takes 12.16 days and requires 18.31 m/s, partitioned into 1.64 m/s and 16.67 m/s for the two impulses, respectively. As shown in the figure, the local evolution of the quasi-periodic trajectory gradually approaches the ideal Halo orbit while the transfer happens. This is direct result of the solar acceleration, which, combined with the gravitational force of the primaries, pushes its evolution rightward. During this time, the spacecraft leaves its E2H section and begins the QH transfer. Since the solar perturbation is not strong enough to cause significant deviation within the short transfer time, the encounter at the second maneuvering point

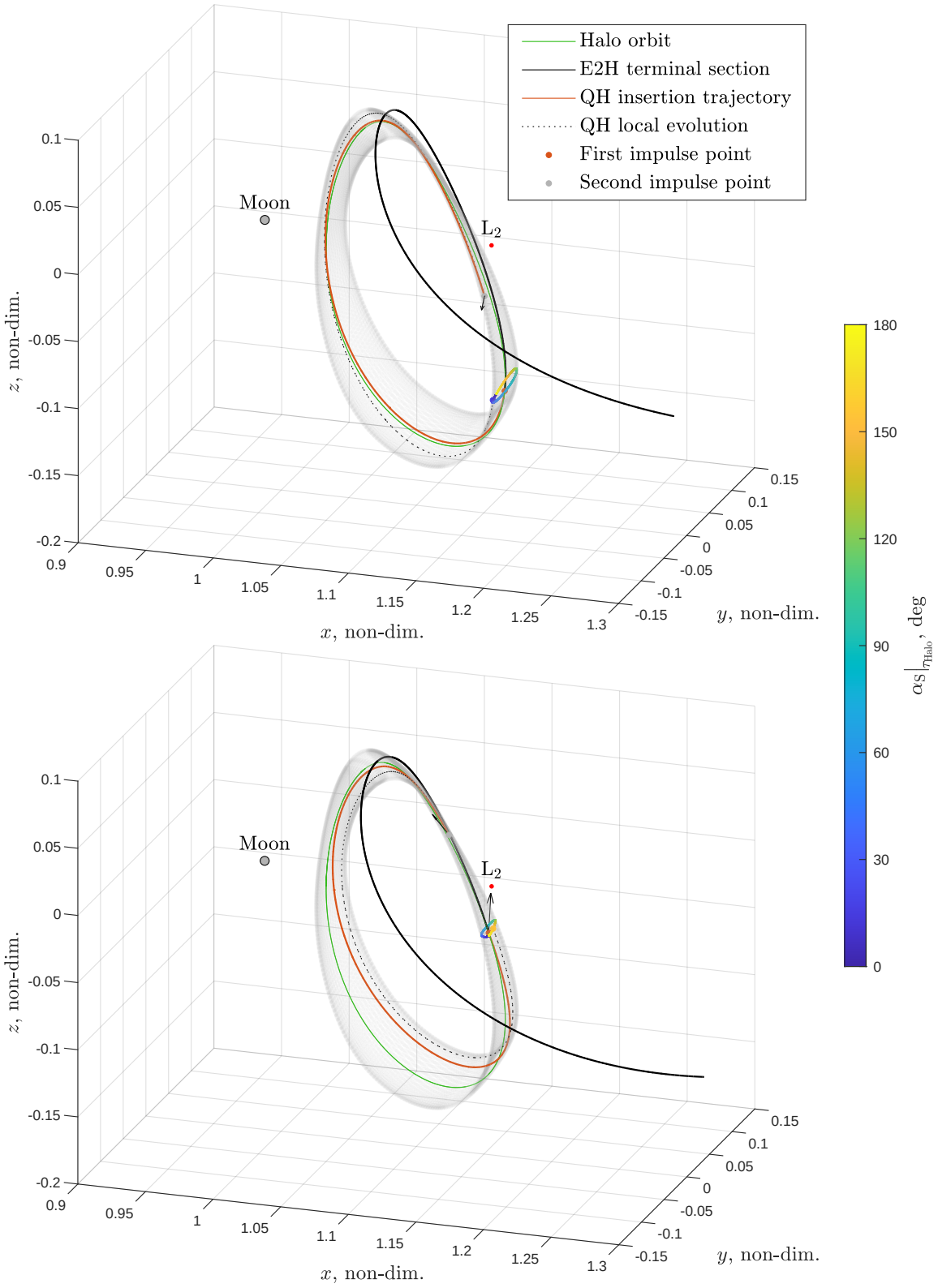

Figure 14: QH insertion phase for solutions highlighted in Figure 13. The transfer experiencing a more efficient injection is reported in the upper tile. In this case, the local quasi-periodic orbit approaches the Halo, thereby reducing the injection cost. Impulsive ΔV vectors are shown as arrows. For a detailed description of the plots refer to the text.

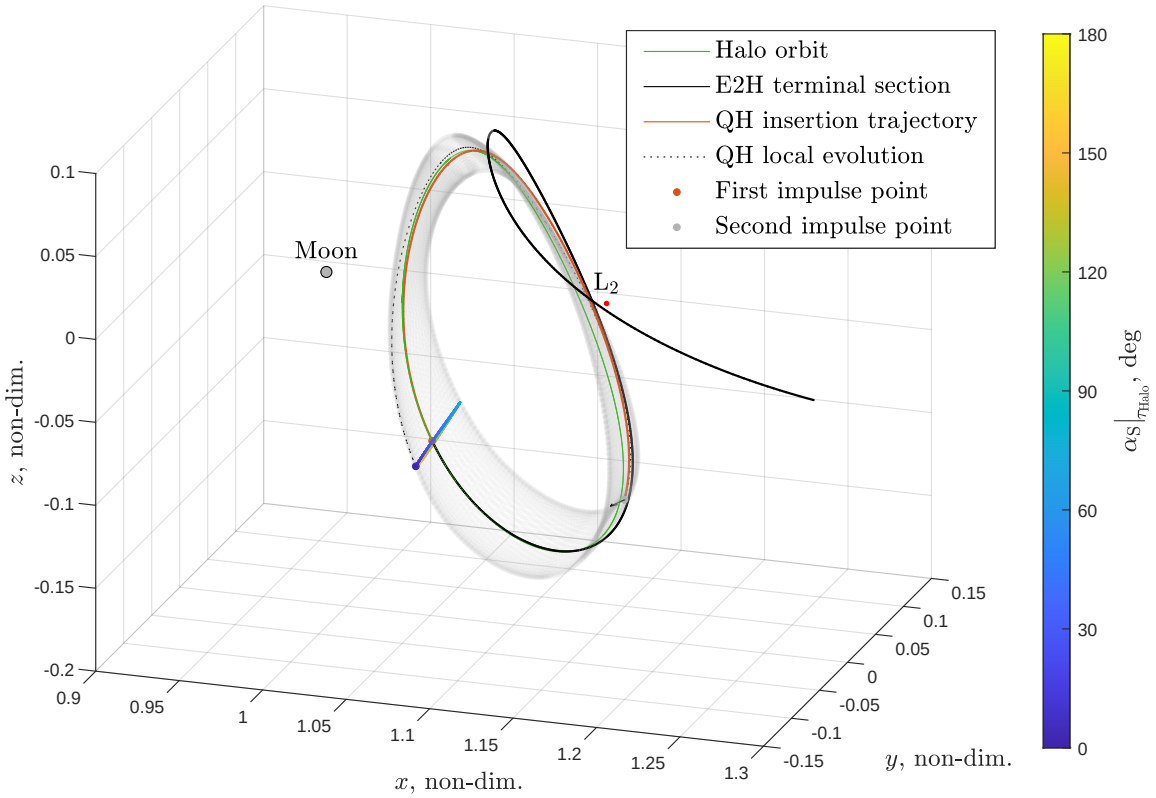

Figure 15: QH insertion phase for the most propulsively efficient Earth-to-QH transfer from the payload perspective. Corresponding E2H section is represented in Figure 7.

occurs at close proximity of the Halo orbit. Then, the second, and more expensive, maneuver is required to instantaneously vary the velocity and equal that of the QH trajectory. In a similar fashion, the lower tile of Figure 14 represents the injection phase of the solution requiring a higher first maneuver propulsive cost. In this case, the QH trajectory emerges and remains apart from the ideal Halo during the entire transfer ($\alpha_S|_{\tau_{Halo}} = 153.99°$). As a result, the spacecraft requires additional fuel to inject itself into the correct path that, eventually, permits inserting into the quasi-periodic orbit. This second example features a transfer duration of 12.44 days and the two impulses expend 34.85 m/s and 19.06 m/s respectively, with a total cost of 53.91 m/s. In general, as the "solar circle" deforms and rotates when varying $\theta|_{\tau_{Halo}}$ and, consequently, generated QHs change, the optimization algorithm converges to solutions whose performance is function of the conditions at the end of the E2H transfer phase. The duration of a QH insertion is then optimized to ensure proper conditions at the execution time of the second maneuver. Figure 12 evidences that short lasting transfers exhibit intermediate costs. No particular relations between conditions emerge in this case.

To conclude this analysis, Figure 15 reproduces the terminal phase of the Earth-to-QH trajectory whose total cost, given by the sum of all DSMs of its E2H phase and the last two impulses necessary to make the QH transfer, is the least among all converging solutions. The first section of the trajectory results to be the one reported in Figure 7. This confirms the impact the optimization of the first section has on the overall design process. The QH transfer and insertion phase solely requires 22.52 m/s and takes 9.23 days, whilst the total cost of the mission is 22.64 m/s.

CONCLUSIONS

The cislunar space is foreseen to play a pivotal role in the next generation of space exploration and exploitation. Additionally, there is a growing trend toward the use of smaller platforms, which enhance the economic appeal of space applications. However, this shift of paradigm introduces technological limitations, leading to stricter mission constraints. Therefore, mission design practices must be carefully tailored to address these challenges.

This paper presents a procedure to generate efficient exterior transfers from Earth to a Quasi-Halo orbit. The trajectory design is divided into two sections. The first stage focuses on achieving an efficient trajectory that departs from a Low Earth Orbit and approaches a Halo orbit about the L_2 point of the Earth–Moon system. Multi-impulse trajectories are optimized within a Sun-perturbed environment, and the number of intermediate maneuvers is varied to assess their impact on overall performance. The second phase involves optimizing the last two impulses required to place the spacecraft into the Quasi-Halo orbit generated from the final conditions of the first transfer section.

The results demonstrate that efficiency can be achieved by leveraging the solar attraction, and its influence is discussed. Performance varies depending on the Sun–Earth–Moon geometrical configuration during the transfer. In light of this, eight initial families of trajectories are identified, covering a broad range of alternatives. Overall, the results show that a spacecraft can successfully establish a Quasi-Halo orbit about L_2 point in an effective manner.

REFERENCES

[1] V. Di Tana, B. Cotugno, S. Simonetti, G. Mascetti, E. Scorzafava, and S. Pirrotta, "ArgoMoon: There is a nano-eyewitness on the SLS," *IEEE Aerospace and Electronic Systems Magazine*, Vol. 34, apr 2019, pp. 30–36, 10.1109/MAES.2019.2911138.

[2] B. Cheetham, "Cislunar Autonomous Positioning System Technology Operations and Navigation Experiment (CAPSTONE)," *ASCEND 2021*, American Institute of Aeronautics and Astronautics, nov 2021, 10.2514/6.2021-4128.

[3] R. Funase *et al.*, "Mission to Earth–Moon Lagrange point by a 6U CubeSat: EQUULEUS," *IEEE Aerospace and Electronic Systems Magazine*, Vol. 35, mar 2020, pp. 30–44, 10.1109/MAES.2019.2955577.

[4] D. A. Dei Tos and F. Topputo, "On the advantages of exploiting the hierarchical structure of astrodynamical models," *Acta Astronautica*, Vol. 136, jul 2017, pp. 236–247, 10.1016/j.actaastro.2017.02.025.

[5] F. Topputo, M. Vasile, and F. Bernelli-Zazzera, "Low energy interplanetary transfers exploiting invariant manifolds of the restricted three-body problem," *The Journal of the Astronautical Sciences*, Vol. 53, dec 2005, pp. 353–372, 10.1007/bf03546358.

[6] W. S. Koon, M. W. Lo, J. E. Marsden, and S. D. Ross, "Low energy transfer to the Moon," *Celestial Mechanics and Dynamical Astronomy*, Vol. 81, No. 1/2, 2001, pp. 63–73, 10.1023/a:1013359120468.

[7] C. T. Campana, G. Merisio, and F. Topputo, "Low-energy Earth–Moon transfers via Theory of Functional Connections and homotopy," *Celestial Mechanics and Dynamical Astronomy*, Vol. 136, May 2024, 10.1007/s10569-024-10192-5.

[8] C. T. Campana and F. Topputo, "On the refinement of low-energy Earth–Moon transfer families into an ephemeris model," *75th International Astronautical Congress (IAC 2024)*, 2024, pp. 1–13.

[9] W. S. Koon, M. W. Lo, J. E. Marsden, and S. D. Ross, *Dynamical systems, the three-body problem and space mission design*. Marsden Books, 2011.

[10] F. Topputo *et al.*, "Meteoroids detection with the LUMIO lunar CubeSat," *Icarus*, Vol. 389, jan 2023, p. 115213, 10.1016/j.icarus.2022.115213.

[11] E. Belbruno, M. Gidea, and F. Topputo, "Weak stability boundary and invariant manifolds," *SIAM Journal on Applied Dynamical Systems*, Vol. 9, jan 2010, pp. 1061–1089, 10.1137/090780638.

[12] R. Castelli, "Regions of prevalence in the coupled restricted three-body problems approximation," *Communications in Nonlinear Science and Numerical Simulation*, Vol. 17, No. 2, 2012, pp. 804–816, 10.1016/j.cnsns.2011.06.034.

[13] J. T. Betts, "Survey of numerical methods for trajectory optimization," *Journal of Guidance, Control, and Dynamics*, Vol. 21, mar 1998, pp. 193–207, 10.2514/2.4231.

[14] B. P. McCarthy and K. C. Howell, "Four-body cislunar quasi-periodic orbits and their application to ballistic lunar transfer design," *Advances in Space Research*, Vol. 71, Jan. 2023, pp. 556–584, 10.1016/j.asr.2022.09.020.

[15] À. Jorba and J. Villanueva, "On the persistence of lower dimensional invariant tori under quasi-periodic perturbations," *Journal of Nonlinear Science*, Vol. 7, Sept. 1997, pp. 427–473, 10.1007/s003329900036.

[16] N. Baresi, Z. P. Olikara, and D. J. Scheeres, "Fully numerical methods for continuing families of quasi-periodic invariant tori in astrodynamics," *The Journal of the Astronautical Sciences*, Vol. 65, Jan. 2018, pp. 157–182, 10.1007/s40295-017-0124-6.

[17] D. Villegas-Pinto, N. Baresi, S. Locoche, and D. Hestroffer, "Resonant quasi-periodic near-rectilinear Halo orbits in the elliptic-circular Earth-Moon-Sun problem," *Advances in Space Research*, Vol. 71, Jan. 2023, pp. 336–354, 10.1016/j.asr.2022.08.011.

[18] D. A. Dei Tos and F. Topputo, "Trajectory refinement of three-body orbits in the real solar system model," *Advances in Space Research*, Vol. 59, apr 2017, pp. 2117–2132, 10.1016/j.asr.2017.01.039.

[19] C. Circi and P. Teofilatto, "On the dynamics of weak stability boundary lunar transfers," *Celestial Mechanics and Dynamical Astronomy*, Vol. 79, No. 1, 2001, pp. 41–72, 10.1023/a:1011153610564.